

Angle-resolved photoemission study and first principles calculation of the electronic structure of GaTe

J.F. Sánchez-Royo

ICMUV, Univ. de Valencia, c/Dr. Moliner 50, 46100 Burjassot, Valencia, Spain
LURE, Centre Universitaire Paris-Sud, Bât. 209 D, B.P. 34, 91898 Orsay Cedex, France

J. Pellicer-Porres, A. Segura, and V. Muñoz-Sanjosé

ICMUV, Univ. de Valencia, c/Dr. Moliner 50, 46100 Burjassot, Valencia, Spain

G. Tobías, P. Ordejón, and E. Canadell

ICMAB, CSIC, Campus de la Univ. Autònoma de Barcelona, 08193 Bellaterra, Barcelona, Spain

Y. Huttel

LURE, Centre Universitaire Paris-Sud, Bât. 209 D, B.P. 34, 91898 Orsay Cedex, France

(October 22, 2018)

The electronic band structure of GaTe has been calculated by numerical atomic orbitals density-functional theory, in the local density approximation. In addition, the valence-band dispersion along various directions of the GaTe Brillouin zone has been determined experimentally by angle-resolved photoelectron spectroscopy. Along these directions, the calculated valence-band structure is in good concordance with the valence-band dispersion obtained by these measurements. It has been established that GaTe is a direct-gap semiconductor with the band gap located at the Z point, that is, at Brillouin zone border in the direction perpendicular to the layers. The valence-band maximum shows a marked p -like behavior, with a pronounced anion contribution. The conduction band minimum arises from states with a comparable s - p -cation and p -anion orbital contribution. Spin-orbit interaction appears to specially alter dispersion and binding energy of states of the topmost valence bands lying at Γ . By spin-orbit, it is favored hybridization of the topmost p_z -valence band with deeper and flatter p_x - p_y bands and the valence-band minimum at Γ is raised towards the Fermi level since it appears to be determined by the shifted up p_x - p_y bands.

PACS numbers: 71.20.Nr, 79.60.Bm

I. INTRODUCTION

Layered materials of the III-VI family like GaSe, InSe, and GaTe are of special interest for their potential applications in nonlinear and optical bistable devices,^{1,2} as well as in the development of solar cells and solid-state batteries.³⁻⁶ Among these compounds, GaTe is one of the less studied because it presents a higher anisotropic and more complex crystal structure than the rest of the III-VI materials. GaTe belongs to the B2/m space group and has a base centered monoclinic unit cell.⁷ The layer structure [see Fig. 1(a)], as that of GaSe or InSe, is composed of a four-sheet anion-cation-cation-anion intralayer stacking pattern in which the bonds are mainly covalent with some ionic contribution. Nevertheless, in contrast to GaSe and InSe, one-third of the cation-cation bonds in GaTe lies almost in the layer plane in a direction perpendicular to the c axis. Differences also exist when considering layer stacking sequences. Similarly to the rest of III-VI compounds, interlayer anion-anion bonds in GaTe are of weak van der Waals type. Generally, this fact promotes the existence of polytypes with different stacking sequences, as is observed in InSe and GaSe.^{8,9} Nevertheless, no polytypism seems to occur in GaTe, as is suggested by the absence of conjugate modes in Raman-

scattering and infrared-absorption measurements.¹⁰ The whole structure gives rise to fourfold coordination for the Ga atoms, with three Te and one Ga atoms, and to threefold coordination for the Te with Ga atoms. As a consequence of these differences in the crystal structure of GaTe with respect to other layered compounds, GaTe has only one twofold symmetry axis, lying along the c axis, whereas other III-VI compounds have a threefold symmetry axis perpendicular to the layer plane.

Besides the common in-plane-out-of-plane anisotropy observed in the optical and electrical properties of the layered compounds, the special in-plane anisotropy in bonding in GaTe makes the optical properties also anisotropic in the layer plane. GaTe is a direct-gap semiconductor with strong excitonic absorption even at room temperature.¹¹⁻¹⁴ The optical properties near the band-gap energy region appear to be slightly anisotropic.¹² Anisotropy of the absorption coefficient has been observed to increase at higher energies, which was attributed to transitions from deep states related to the in-plane Ga-Ga bonds.¹⁴ Moreover, low-temperature photoluminescence and transmission measurements revealed the presence of different exciton states depending on the in-plane polarization vector.¹⁵ Recently, these results were explained by the existence of three types of exciton

states due to j - j coupling, whose optical transitions are allowed under the group symmetry of this material.¹⁶

There is still a lack of both theoretical and experimental studies on the electronic band structure of GaTe. One of the reasons for this lacuna lies on the complexity of the primitive unit cell, that contains 6 GaTe units (54 valence electrons), which has made band structure calculations hardly available up to now. Recently, the electronic band structure of GaTe has been calculated along some directions by the *ab initio* tight-binding linear muffin-tin orbitals method.¹⁶ These results are in agreement with the direct-gap behavior of this semiconductor and locate the band edge at the border of the Brillouin zone (BZ). Nevertheless, there are still some open questions regarding the electronic band structure along the high-symmetry directions of the GaTe BZ, as well as the experimental confirmation of the electronic band structure obtained in the calculations.

In this work we study the electronic properties of the GaTe compound. The GaTe band structure has been calculated by numerical atomic orbitals density-functional theory (NAO-DFT). In addition, angle-resolved photoemission (ARPES) measurements have been carried out in GaTe(001) single crystals. From these measurements, the valence-band dispersion of GaTe was extracted and interpreted on the basis of the band structure calculations. The experimental setup is described in Sec. II. Section III is devoted to the band structure of GaTe calculated along different directions of the GaTe BZ, including the technical aspects of the calculation. In Sec. IV, the experimental results obtained by ARPES are presented and discussed in the frame of the calculated GaTe band structure. Finally, in Sec. V we present the main conclusions of this work.

II. EXPERIMENTAL

The experiments were performed at LURE (Orsay, France) using the Spanish-French (PES2) experimental station of the Super-Aco storage ring, described elsewhere.¹⁷ The measurements were carried out in a purpose-built ultra-high vacuum system, with a base pressure of 5×10^{-11} mbar, equipped with an angle resolving 50 mm hemispherical VSW analyzer coupled on a goniometer inside the chamber. The manipulator was mounted in a two-axes goniometer which allows rotation of the sample in the whole 360° azimuthal angle and in the 180° polar emission angle relative to surface normal (Θ_{off}), with an overall angular resolution of 0.5° . Photoelectrons were excited with p-polarized synchrotron radiation in the 20-60 eV energy range. For this selected photon energy ($h\nu$) range, the energy resolution was of 60 meV. With this setup, different energy-distribution-curve (EDC) series were recorded scanning the $h\nu$ as well as Θ_{off} , at constant incident angle of the light (Θ_i). In these conditions, changes of polarization effects on ini-

tial states along one series are neglected. All the EDC spectra shown in this work are referred to the Fermi level (E_F).

The GaTe single crystals used in this work were cut from an ingot grown by the Bridgman-Stockbarger method. The samples were cleaved *in situ* after introduction in the ultra-high vacuum chamber. The samples were easily cleaved in the layer plane due to the existence of weak interlayer van der Waals bonds. LEED spectra showed a sharp spot pattern corresponding to the bulk monoclinic material. No surface impurities were detected by synchrotron radiation photoemission measurements. The samples were oriented by azimuthal and polar photoelectron diffraction scans recording the Ga 3d peak intensity. Unambiguous azimuthal orientation of the samples was possible due to the B2/m symmetry of the crystal.

III. BAND STRUCTURE OF GATE

A. Calculation details

In this work, we present fully self-consistent density-functional theory¹⁸ (DFT) calculations of the electronic structure of GaTe. The calculations are performed in the local-density approximation.¹⁹ The exchange-correlation potential is that of Ceperley and Adler²⁰ as parameterized by Perdew and Zunger.²¹ Only the valence electrons are considered in the calculation, with the core being replaced by norm-conserving scalar relativistic pseudopotentials²² factorized in the Kleinman-Bylander form.²³ The pseudopotentials were generated using the atomic valence configurations $5s^25p^4$ for Te and $3d^{10}4s^24p^1$ for Ga. The cutoff radii were 2.0, 2.0, 3.0, and 3.0 a.u. for the s , p , d , and f components in Te, respectively, and 2.1, 2.3, 1.1 and 2.0 a.u. for the s , p , d , and f components of Ga, respectively. Since the core and valence charges overlap significantly for both atomic species, we include nonlinear partial-core corrections²⁴ with matching radii of 1.0 a.u. for Te and 0.5 a.u. for Ga to describe the exchange and correlation in the core region.

The valence one-particle problem was solved using a linear combination of numerical (pseudo-) atomic orbitals with finite range.²⁵ The details of the basis generation (including multiple- ζ and polarization functions) can be found elsewhere.²⁶ In this work we have used a split-valence double- ζ basis set with a single shell of polarization orbitals (that is, containing two s shells, two p shells, and one d shell both for Te and for Ga), as obtained with an energy shift of 250 meV and a split norm of 15%.²⁶ The integrals of the self-consistent terms of the Kohn-Sham Hamiltonian are obtained with the help of a regular real space grid on which the electron density is projected. The Hartree potential is calculated by means of fast Fourier transforms in that grid. The grid spacing is determined by the maximum kinetic energy of the

plane waves that can be represented in that grid. In the present work, we used a cutoff of around 300 Ry (which changes slightly with the volume of the unit cell). A regular grid of $5 \times 5 \times 5$ k points²⁷ was used to sample the BZ. We have checked that the results are well converged with respect to the real space grid, the BZ sampling and the range of the numerical atomic orbitals. The calculations were performed using the SIESTA code.²⁸

In our band structure calculations, we used a centered monoclinic cell with primitive vectors $\mathbf{a}' = -\mathbf{b} + (\mathbf{c} - \mathbf{a})/2$, $\mathbf{b}' = -\mathbf{b} - (\mathbf{a} + \mathbf{c})/2$, and $\mathbf{c}' = -\mathbf{b}$, where \mathbf{a} , \mathbf{b} , and \mathbf{c} are the repeat vectors of the monoclinic cell [see Figure 1(a)]. Note that, with this election, \mathbf{a}' and \mathbf{b}' vectors are in the layer plane.

B. Brillouin zone and electronic band structure

Figure 1(a) shows the crystal structure of GaTe, described previously. In this figure, we have indicated the crystallographic axes of the GaTe monoclinic unit cell. The GaTe crystal structure is quite similar to those of GaSe and InSe, except for the existence of cation-cation bonds lying almost in the layer plane, with the same coordination and bonding behavior. The comparison can be also extended to the reciprocal space. Figure 1(b) shows the calculated GaTe BZ, in which the main points are indicated. The relation between the different symmetry directions of the GaTe BZ and the reciprocal lattice vectors of the centered monoclinic unit cell is shown in Table I.

The GaTe BZ can be easily described in terms of the crystal structure. The binary axis corresponds to the ΓY high-symmetry direction and a crystal vector perpendicular to the layer plane defines a direction parallel to the ΓZ high-symmetry direction, in the reciprocal space. The GaTe BZ resembles that of InSe, but contracted along the ΓX direction. The contraction is due to the presence of the *quasi*-in-plane Ga-Ga bonds in GaTe, which produces that the fundamental translation in the layer plane consists of three Ga_2Te_2 unities, in contrast to one unity in the other III-VI compounds. On the other side, as both GaTe and InSe have only one layer per unit cell, one should expect the electronic band structure of GaTe to be related to that of InSe, after a three-folding in the layer plane.

Figure 2 shows the electronic band structure of GaTe along different directions of the GaTe BZ [Fig. 1(b)] calculated by the NAO-DFT method described previously. The origin of binding energy has been taken at the E_F . In spite of the large number of bands obtained, a detailed description of the valence band can be done. The GaTe unit cell consists of three Ga_2Te_2 unities. Therefore, there are per unit cell: three Ga-Ga bonds, 18 Ga-Te bonds, and one electronic pair associated to each one of the six Te. This gives rise to 27 doubly occupied bands, which are precisely those appearing with binding energies

between 14 eV and E_F and composing the GaTe valence band. Below this energy (at 16.5 eV), the $3d$ -core levels of Ga are present (not shown). The unoccupied side of the band structure is rather more complicated to be described, since, besides the 18 Ga-Te and 3 Ga-Ga antibonding levels, all contributions from the polarization d -orbitals overlap.

A detailed band to band description of the band structure of GaTe would not be very useful due to the fact that the low symmetry of the crystal makes the orbital mixture of each band to be very high. Nevertheless, a general description of the orbital character of the GaTe band structure can be performed by means of the density of states (DOS). Figure 3(a) shows the total DOS calculated by the NAO-DFT method. Figure 3(b) and 3(c) show the different projections of the s , p , and d orbitals onto the DOS for Ga and Te, respectively. These results indicate that the valence band of GaTe can be divided into three different groups: (i) One group of six bands appearing between 14 and 11 eV, which show a pronounced Te $5s$ relative behavior with a small Ga $4s$ and $4p$ contribution, (ii) a second group of six bands appearing between 8 and 5 eV, which mostly show a Ga $4s$ character with a pronounced Te $5p$ contribution in the low binding energy side, and (iii) a third group of 15 bands comprising the range of energy between 5 eV and the E_F , which are a mixture of Te $5p$ and Ga $4p$ orbitals with a small Ga $4d$ and $4s$ contribution. The origin of these groups differs from one to the other. On one side, the first and second group of bands appear to be mostly originated by the Ga-Te bonds, showing those with a marked p -like behavior a more pronounced dispersion along the ΓZ high-symmetry direction (as well as along directions perpendicular to it) than those with a predominant s -like behavior (Fig. 2). On the other side, in the third group of bands, they coexist six bands originated also from the Ga-Te bonds, three bands from the Ga-Ga bonds, and the six electronic pairs associated to the Te (mostly Te $5p$). Focusing our attention on the topmost valence bands, the fact that their orbital character has an important p -like component perpendicular to the layers, makes that most of the bands display a noticeable dispersion along ΓZ high-symmetry direction (Fig. 2).

With regard to the DOS corresponding to the unoccupied side of the band structure, the huge overlap of Ga-Te and Ga-Ga antibonding levels with the d -orbitals of polarization makes an orbital description quite more complicated than that carried out for the occupied side of the DOS. Nevertheless, it should be mentioned that states at the conduction band edge are mostly originated from Te $5p$ and Ga $4p$ orbitals, with an important contribution from Ga $4s$ and a smaller contribution Te $5d$ and Ga $4d$, which suggests a pronounced sp_z -like behavior to the conduction band edge. Only for higher states in the conduction band, contributions from Ga and Te d -orbitals of polarization appear to be of the same magnitude than those of the p -orbitals.

The general shape and the different orbital contributions to the calculated DOS by NAO-DFT are quite similar to those obtained previously by the *ab initio* tight binding method.¹⁶ Some differences can be appreciated in the unoccupied side of the DOS. By both methods, the behavior of the conduction band edge seems to be established as a mixture of *s* and *p* orbitals. Nevertheless, in contrast to previous calculations,¹⁶ the Ga *4p* contribution to the conduction band edge appears to be of the same order as that of the Ga *4s*, which gives a more pronounced *p*-like behavior to the conduction band edge in the present calculations. Also the contribution of Ga and Te *d*-orbitals of polarization to the conduction band edge, as well as to deeper states of the conduction band, seem to be underestimated in those calculations (mostly the Ga *4d*). As regards the band dispersion, authors seem to have used a standard six-face monoclinic BZ,¹⁶ which does not correspond to the GaTe BZ. The band dispersion calculated along some directions in Ref. 16 (see Table I) is very similar to the present results. However, along other directions, as the ΓZ and AM directions in Fig. 8 of Ref. 16, the path crosses out of the first BZ to neighboring ones, giving rise to the *quasi*-symmetrical band dispersion observed along these directions.

From the above results, it can be concluded that GaTe is a direct-gap semiconductor with the gap located at zone border at Z point of the GaTe BZ, which has the same symmetry as Γ (B2/m). The band gap appears to be underestimated (1.098 eV), which is a well-known tendency of the LDA approximation in semiconductors. As in InSe,²⁹ the valence-band maximum is mostly formed by antibonding *p_z*-orbitals of the anion. Nevertheless, in contrast to InSe,²⁹ the conduction-band minimum is not only formed by the *s*-orbital contribution of the cation. In GaTe a more intense contribution of cation and anion *p*-orbitals can be observed. This can be attributed to the fact that the presence of the *quasi*-in-plane cation-cation bonds distorts the anion disposition and, therefore, the interaction of Te atoms with those of contiguous layers and with Ga atoms increases.

IV. EXPERIMENTAL RESULTS AND DISCUSSION

In this section, we compare the calculated electronic band structure of GaTe with the band dispersion determined experimentally by ARPES in GaTe(001) single crystals. First, we will show and discuss the electronic band dispersion along the ΓZ high-symmetry direction, proceeding later with those determined along different directions perpendicular to it.

Figure 4(a) shows an EDC series recorded at normal emission with constant Θ_i in a GaTe(001) sample, as a function of the $h\nu$. In these spectra, several peaks have been identified and labelled by small solid bars. In some of them, two sharp dispersing peaks can be also observed,

which can be attributed to second-order transitions from deeper occupied states induced by the experimental system. As the $h\nu$ increases, these sharp peaks move to lower binding energies. Therefore, photoemission signal from deeper valence-band transitions than those of Fig. 4(a) can be studied in EDCs recorded by extending up the $h\nu$ -range of Fig. 4(a). Figure. 4(b) shows the results of these measurements. In these spectra, only broad features can be identified, at binding energies of 12.6 eV, which have been labelled as *s-band*.

By these results, the dispersion of states along the ΓZ high-symmetry direction can be determined. Nevertheless, to compare these results with the calculated band structure, the momentum of photoelectrons should be estimated. Photoemission process involves energy and crystal momentum conservation. In the frame of the three-step model of the photoexcitation mechanism in ARPES, both momentum components, k_{\parallel} and k_{\perp} , of the photoelectrons inside a bulk material can be expressed as³⁰

$$k_{\parallel} = \sqrt{\frac{2m}{\hbar^2}} \sqrt{h\nu - BE - \Phi} \sin(\Theta_{off}) \quad (1a)$$

and

$$k_{\perp} = \sqrt{\frac{2m}{\hbar^2}} \sqrt{(h\nu - BE - \Phi) \cos^2(\Theta_{off}) - V_o}, \quad (1b)$$

where BE is the binding energy, Φ is the work function, V_o is the inner potential, m is the free-electron mass, and \hbar is the reduced Planck constant. A complete determination of the photoelectron momentum requires an accurate estimate of the V_o [Eq.(1b)]. We have assumed it as a constant parameter. An initial testing value of $V_o \sim -19$ eV ($\Phi \sim 6$ eV) can be obtained from the bottom of the valence band (Fig. 2). After testing several values of V_o and taking into account that $k_{\Gamma Z} = 0.421 \text{ \AA}^{-1}$, we have adopted a value of $V_o = -25.7$ eV, which is two times higher than that found for InSe.³¹ Such a high value of the V_o for GaTe is not surprising, since the orbital hybridization giving rise to the GaTe valence-band structure is higher than in InSe. In any case, it is reasonably close to the value expected from the valence-band calculations.

Figure 4(c) shows the valence-band dispersion extracted from the peaks identified in Fig. 4(a), by means of Eqs. (1). The calculated valence-band dispersion along the ΓZ high-symmetry direction has been also included. In spite of the large number of different bands present, it can be observed that the calculated band structure reproduces most of the traces observed in the experimental band dispersion. The large concentration of quite flat bands appearing at lower binding energies is well reproduced by the calculated valence-band structure, with states lying at similar binding energies. These facts also put forward the highly hybridized behavior of top states of the valence-band structure predicted by calculations (Fig. 2). Besides this, dispersion of states with a marked

Te $5p$ -Ga $4s$ orbital character (that is, states between 8 and 5 eV in binding energy) is quite well reproduced. Moreover, the presence of the broad *s-band* peaks in Fig. 4(b) can be attributed to transitions from the Te $5s$ -like states, located at binding energies of ~ 12 eV (Fig. 2). Nevertheless, some discrepancies appear for states lying at the top of the valence band. Experimentally, the valence-band maximum along the ΓZ high-symmetry direction appears to be at Z point and the minimum of the valence-band lies at Γ . These facts are in concordance with the calculated valence-band structure. Moreover, dispersion of the topmost band around Z is well reproduced by the calculations. However, the valence-band minimum at Γ obtained by calculations appears shifted down by 0.8 eV with respect to the experimental one. A similar situation occurs with the second topmost valence band. For this band, the calculated band minimum, also at Γ , appears to be shifted down by 0.6 eV with respect to the experimental one. This disagreement will be discussed later on.

Figure 5(a) shows an EDC series measured by ARPES with $h\nu=33$ eV in a GaTe(001) sample. The sample orientation has been chosen to probe, by these ARPES measurements, points of the reciprocal space contained in the ΓZH plane. In fact, for this selected $h\nu$, these points are expected to have a k_{\perp} lying quite close to the Z point [Eqs.(1)]. In the spectra shown in Fig. 5(a), several peaks have been identified and labelled by small solid bars. Figure 5(b) shows the band dispersion extracted from the peaks identified in Fig. 5(a).

In order to compare the experimental band dispersion shown in Fig. 5(b) with the calculated band structure, it should be taken into account that, by the ARPES measurements summarized in Fig. 5(a), particular points of the reciprocal space along a parabolic curve are probed for each constant initial state [Eqs. (1)]. For initial states with low binding energy, the minimum of the parabola will be close to the Z point, but when running from Z to H ($k_{ZH}=0.744 \text{ \AA}^{-1}$) the parabolic curve perpendicularly deviates from horizontality by 0.07 \AA^{-1} . For deeper initial states, the parabolas probe points somewhere along the ΓZ high-symmetry direction. These facts produce that, by these measurements, states along the ZH direction are not strictly probed. Nevertheless, it has been found that dispersion of valence-band states along the ΓZ high-symmetry direction can be considered negligible in a large k_{\perp} -range [Fig. 4(c)]. These facts encourages us to assume that the calculated band structure along the ZH direction is a good approximation for the experimental band dispersion, as shown in Fig. 5(b). In this figure, it has been also introduced the calculated band dispersion of states with binding energies higher than 3 eV along the ΓY high-symmetry direction, which is not far from that calculated along the ZH direction and gives a better agreement with the experimental band dispersion of deeper bands.

Figure 6(a) and 6(b) show two different EDC series measured by ARPES with $h\nu=33$ eV in a GaTe(001)

sample. In these ARPES measurements, a sample orientation has been chosen to probe points of the reciprocal space contained in the ΓZM plane. In these spectra, several peaks have been identified and labelled by small solid bars. Figure 6(c) shows the ΓZM transversal cut of the GaTe BZ, in the extended zone scheme. The parabolic curve defined by ARPES measurements with $h\nu=33$ eV for constant initial states at the E_F is also included in this figure. This scheme illustrates the fact that, by both sets of measurements shown in Figs. 6(a) and 6(b), points of the reciprocal space are probed along the MZM' and $MG'M'$ directions, respectively. Figure 6(d) shows the band dispersion extracted from the peaks identified in Figs. 6(a) and 6(b). Assuming the same hypotheses as those discussed previously, we have also included the calculated band dispersion along the MZM' and $MG'M'$ directions, which reproduce most of the traces of the band dispersion obtained experimentally. Focusing again attention on the two topmost valence-bands, their dispersion around Z along the MZM' direction appears to be rather flat, coherently with the behavior expected by NAO-DFT calculations. Nevertheless, dispersion of these bands along the $MG'M'$ direction shows the same behavior as that observed along the ΓZ high-symmetry direction [Figs. 4(c)], with the same separation at Γ between the calculated and experimental minimums of these bands.

The above results obtained by ARPES measurements along different directions of the GaTe BZ support the results obtained by NAO-DFT band structure calculations (Fig. 2). Among these results, it should be emphasized the fact that experimental and calculated band structure place the valence-band maximum in GaTe at zone border at Z, similarly as occurs in the InSe compound.²⁹ Nevertheless, despite the good agreement obtained through the whole reciprocal space studied, there still remains one point of discrepancy related to the two topmost valence-bands at Γ [Figs. 4(c) and 6(d)], since the binding energy of the minimum of these bands appear to be overestimated by calculations. These facts can be explained since spin-orbit interaction was not considered in the present calculations. In the related compound InSe, the band giving rise to the valence band maximum at Z mostly has a marked p_z -orbital character. States of this band have a total orbital moment $j=1/2$. Without considering spin-orbit interaction, this band disperses down along the ΓZ direction, showing the minimum at Γ . Below this band, the next ones are quite flat bands with a p_x - p_y character. Spin-orbit interaction splits off p_x - p_y states with different j , rising those with $j=3/2$ by 0.3-0.4 eV,³² with respect to the valence band maximum. This produces that the minimum of the topmost valence band at Γ is determined by the shifted up p_x - p_y bands. A more intense spin-orbit coupling can be expected in GaTe, since the nature of its topmost valence bands is the same as those of InSe and its anion has a higher mass. In fact, the spin-orbit induced shift on the valence-band minimum at Γ in GaTe may be evaluated. Taking into account that the atomic spin-orbit $p_{3/2}$ - $p_{1/2}$ splitting is of 589 and 247 meV for

Te and Se, respectively,³³ in GaTe one should expect a shift up of the $j=3/2$ p_x - p_y bands at Γ of the order of 0.7-0.9 eV, which is close to that observed in Figs. 4(c) and 6(d).

V. CONCLUSIONS

The electronic band structure of GaTe single crystal has been calculated by a NAO-DFT method. These results show that, on one side, the deepest valence bands are mostly formed by Ga-Te orbitals with a marked s -like behavior and, on the other side, bands with a low binding energy have a pronounced p -orbital character originated by cation-anion bonds, as well as by anion electronic pairs and cation-cation bonds. Also, the conduction-band structure was determined. It appears to be composed by bands with mainly a p -orbital character, originated from the antibonding Ga-Te and Ga-Ga bonds, intermixed with the d -orbitals of polarization.

The electronic properties of GaTe single crystal have been studied also by ARPES measurements. By these measurements, dispersion of the valence bands along various directions of the GaTe BZ has been determined. The experimental band dispersion obtained appears to be quite well reproduced by the calculated band dispersion along these directions.

These results establish that GaTe is a direct-gap semiconductor with a gap located at zone border, at Z point. The valence-band maximum shows a marked p -like behavior, with a pronounced anion contribution. The conduction band minimum arises from states with a comparable s - p -cation and p -anion orbital contribution. Spin-orbit interaction appears to specially alter the dispersion and binding energy of states of the topmost valence bands lying at Γ . Spin-orbit favors the hybridization of the topmost p_z -valence band with deeper and flatter p_x - p_y bands. Also, it rises the valence-band minimum at Γ towards the E_F , which appears to be determined by the shifted up $j=3/2$ p_x - p_y bands.

ACKNOWLEDGMENTS

This work was financed by the Large Scale Facilities program of the EU to LURE. The authors gratefully acknowledge Dr. J. Avila and Dr. M.C. Asensio for technical and scientific support at LURE. J.F.S.-R. and G.T. acknowledge financial support from the Ministerio de Educación y Cultura and Ministerio de Ciencia y Tecnología of Spain, respectively. Part of this work was supported by DGI-Spain (Project BFM2000-1312-C02-01), Generalitat de Catalunya (Project 1999SGR207) and Fundación Ramón Areces. The computations were carried out using the resources of CESCO and CEPBA, coordinated by C⁴.

-
- ¹ W. C. Eckhoff, R. S. Putnam, S. Wang, R. F. Curl, and F. K. Tittel, *Appl. Phys. B: Solids Surf.* **63**, 437 (1996).
 - ² M. A. Hernández, J. F. Sánchez, M. V. Andrés, A. Segura, and V. Muñoz, *Óptica Pura y Aplicada* **26**, 152 (1993).
 - ³ J. Martínez-Pastor, A. Segura, J. L. Valdés, and A. Chevy, *J. Appl. Phys.* **62**, 1477 (1987).
 - ⁴ J. F. Sánchez-Royo, A. Segura, O. Lang, E. Schaar, C. Pettenkofer, W. Jaegermann, L. Roa, and A. Chevy, *J. Appl. Phys.* **90**, 2818 (2001).
 - ⁵ V. K. Lukyanyuk, M. V. Tivarnitskii, and Z. D. Kovalyuk, *Phys. Status Solidi A* **104**, K41 (1987).
 - ⁶ M. Balkanski, C. Julien, and J. Y. Emery, *J. Power Sources* **26**, 615 (1989).
 - ⁷ M. Julien-Pouzol, S. Jaulmes, M. Guittard, and F. Alapini, *Acta Crystallogr. B* **35**, 2848 (1979).
 - ⁸ A. Linkforman, D. Carré, J. Etienne, and B. Bachet, *Acta Crystallogr. B* **31**, 1252 (1975); J. Rigoult, A. Rimsky, and A. Kuhn, *Acta Crystallogr. B* **36**, 916 (1980).
 - ⁹ W. Schubert, E. Dörre, and M. Kluge, *Z. Metallk.* **46**, 216 (1955); A. Kuhn, R. Chevalier, and A. Rimsky, *Acta Crystallogr. B* **31**, 2841 (1975); S. Benazeth, N. -H. Dung, M. Guittard, and P. Laruelle, *Acta Crystallogr. C* **44**, 234 (1988); K. Cenzual, L. M. Gelato, M. Penzo, and E. Parthé, *Acta Crystallogr. B* **47**, 433 (1991).
 - ¹⁰ J. C. Irwin, B. P. Clayman, and D. G. Mead, *Phys. Rev. B* **19**, 2099 (1979).
 - ¹¹ J. Camassel, P. Merle, H. Mathieu, and A. Gousskov, *Phys. Rev. B* **19**, 1060 (1979).
 - ¹² J. Camassel, P. Merle, and H. Mathieu, *Physica B* **99**, 309 (1980).
 - ¹³ A. Gousskov, J. Camassel, and L. Gousskov, *Prog. Cryst. Growth Charact.* **5**, 323 (1982).
 - ¹⁴ J. F. Sánchez-Royo, A. Segura, and V. Muñoz, *Phys. Status Solidi A* **151**, 257 (1995).
 - ¹⁵ J. Z. Wan, J. L. Brebner, R. Leonelli, and J. T. Graham, *Phys. Rev. B* **46**, 1468 (1992); J. Z. Wan, F. H. Pollak, J. L. Brebner, and R. Leonelli, *Solid State Commun.* **102**, 17 (1997).
 - ¹⁶ A. Yamamoto, A. Syouji, T. Goto, E. Kulatov, K. Ohno, Y. Kawazoe, K. Uchida, and N. Miura, *Phys. Rev. B* **64**, 035210 (2001).
 - ¹⁷ J. Avila, C. Casado, M. C. Asensio, J. L. Pérez, M. C. Muñoz, and F. Soria, *J. Vac. Sci. Technol. A* **13**, 1501 (1995).
 - ¹⁸ P. Hohenberg and W. Kohn, *Phys. Rev.* **136**, 864 (1964).
 - ¹⁹ W. Kohn and L. J. Sham, *Phys. Rev.* **140**, 1133 (1965).
 - ²⁰ D. M. Ceperley and B. J. Alder, *Phys. Rev. Lett.* **45**, 566 (1980).
 - ²¹ J. P. Perdew and A. Zunger, *Phys. Rev. B* **23**, 5048 (1981).
 - ²² N. Troullier and J. L. Martins, *Phys. Rev. B* **43**, 1993 (1991).
 - ²³ L. Kleinman and D. M. Bylander, *Phys. Rev. Lett.* **48**, 1425 (1982).
 - ²⁴ S. G. Louie, S. Froyen, and M. L. Cohen, *Phys. Rev. B* **26**, 1738 (1982).

- ²⁵ O. F. Sankey and D. J. Niklewski, Phys. Rev. B **40**, 3979 (1989).
- ²⁶ E. Artacho, D. Sánchez-Portal, P. Ordejón, A. García, and J. M. Soler, Phys. Status Solidi B **215**, 809 (1999).
- ²⁷ H. J. Monkhorst and J. D. Pack, Phys. Rev. B **13**, 5188 (1976).
- ²⁸ D. Sánchez-Portal, P. Ordejón, E. Artacho, and J. M. Soler, Int. J. Quantum Chem. **65**, 453 (1997).
- ²⁹ F. J. Manjón, D. Errandonea, A. Segura, V. Muñoz, G. Tobías, P. Ordejón, and E. Canadell, Phys. Rev. B **63**, 125330 (2001).
- ³⁰ S. Hüfner, *Photoelectron Spectroscopy*, Springer Series in Solid-State Sciences n. 82 (Springer-Verlag, Berlin Heidelberg, 1995).
- ³¹ A. Amokrane, F. Proix, S. El Monkad, A. Cricenti, C. Barchesi, M. Eddrief, K. Amimer, and C. A. Sébenne, J. Phys.: Condens. Matter **11**, 4303 (1999).
- ³² P. Gomes da Costa, R. G. Dandrea, R. F. Wallis, and M. Balkanski, Phys. Rev. B **48**, 14135 (1993).
- ³³ *Atomic Energy Levels*, edited by C.E. Moore, Natl. Bur. Stand. (U.S.) Circ. No. 467 (U.S. GPO, Washington, D.C., 1958), Vol. 2 (for Se) and Vol. 3 (for Te).

TABLE I. Main directions of the GaTe Brillouin zone as generated by the reciprocal lattice vectors. These directions have been identified with those defined in Ref. 16 and expressed as a function of the cell vectors (\mathbf{G}_i) there defined.

This work		Ref. 16 ^a	
ΓZ	$\mathbf{c}^*/2$	$\Gamma P(M)$	$(\mathbf{G}_1 + \mathbf{G}_2 - \mathbf{G}_3)/2$
ΓA	$-\mathbf{b}^*/2$	ΓL	$(\mathbf{G}_2 - \mathbf{G}_3)/2$
ΓP	$-(\mathbf{a}^* + \mathbf{b}^*)/2$	ΓX	$(\mathbf{G}_1 + \mathbf{G}_2 - 2\mathbf{G}_3)/2$
ΓN	$-(\mathbf{a}^* + \mathbf{b}^* + \mathbf{c}^*)/2$	ΓA	$-\mathbf{G}_3/2$
ΓB	$(\mathbf{a}^* + \mathbf{c}^*)/2$	ΓV	$\mathbf{G}_2/2$
$\Gamma A'$	$\mathbf{a}^*/2$	ΓL	$(\mathbf{G}_3 - \mathbf{G}_1)/2$

^a $\mathbf{G}_1 = \mathbf{b}^* + \mathbf{c}^*$, $\mathbf{G}_2 = \mathbf{a}^* + \mathbf{c}^*$, and $\mathbf{G}_3 = \mathbf{a}^* + \mathbf{b}^* + \mathbf{c}^*$.

FIG. 1. (a) Schematic view of the crystal structure of GaTe and its monoclinic unit cell. Non-equivalent atoms have different shadowing. Big and small circles correspond to Te and Ga atoms, respectively. (b) GaTe centered monoclinic Brillouin zone, in which the main points are indicated. Equivalent Q-points (Q generic) have been labelled as Q', Q'', and so forth. The ΓXY plane is parallel to the layers and the ΓY direction corresponds to the binary axis. The ΓZX plane defines the mirror plane.

FIG. 2. Band structure of GaTe calculated by the NAO-DFT method along various directions of the GaTe BZ.

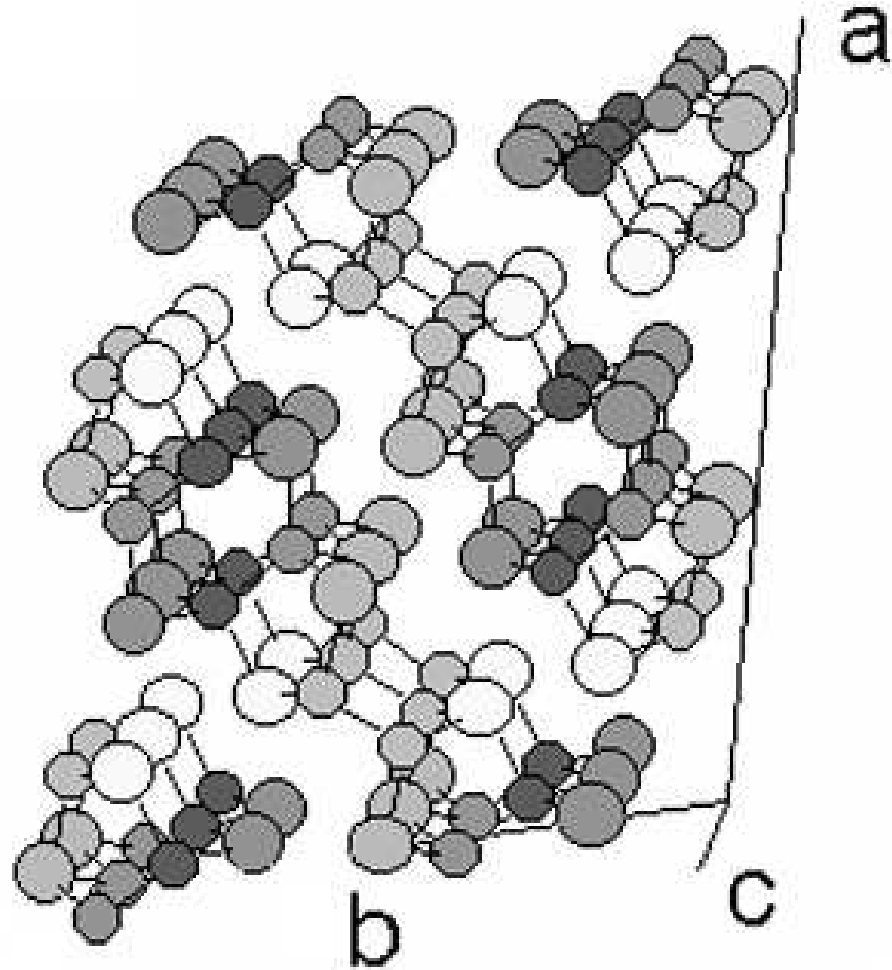
FIG. 3. (a) Density of states of GaTe. (b)-(c) Projections of the s , p , and d orbitals onto the total density of states, for Ga and Te, respectively.

FIG. 4. (a)-(b) Normal-emission valence-band EDCs measured in GaTe(001) single crystal, as a function of the $h\nu$. The $h\nu$ range scanned has been indicated in both figures. The different peaks identified in the EDCs in (a) have been marked by small solid bars. The broad peaks identified in the EDCs in (b) have been labelled as *s-band*. (c) (circles) Band dispersion diagram extracted from the peaks identified in (a). The calculated GaTe band structure along the $Z\Gamma Z$ high-symmetry direction has been also plotted, in solid lines.

FIG. 5. (a) Valence-band EDCs measured by ARPES with $h\nu=33$ eV in GaTe(001) single crystal. For this selected $h\nu$, the ZH direction is scanned by ARPES. The different peaks identified have been marked by small solid bars. (b) (circles) Band dispersion diagram extracted from the peaks identified in (a). The calculated GaTe band structure along the ZH direction has been also plotted, in solid lines. The calculated band dispersion of states with binding energies higher than 3 eV along the ΓY high-symmetry direction has been also plotted, in dashed lines. As a reference, the k_{\parallel} -projection of some points of the GaTe BZ are indicated at the top.

FIG. 6. (a) Valence-band EDCs measured by ARPES with $h\nu=33$ eV in GaTe(001) single crystal. For this selected $h\nu$, the ZM direction is scanned by ARPES. (b) The same that (a) extending the Θ_{off} -range to scan the MGM' direction. In both EDC series, the different peaks identified have been marked by small solid bars. (c) Schematic view of the BZ cut with the ΓZM plane. The parabolic curve defined by ARPES measurements with $h\nu=33$ eV for constant initial states at the E_F is also included. (d) (circles, squares) Band dispersion diagram extracted from the peaks identified in (a) and (b), respectively. The calculated GaTe band structure along the MZM' and MGM' directions has been also plotted, in solid lines. As a reference, the k_{\parallel} -projection of some points of the GaTe BZ are indicated at the top.

(a)



(b)

